IBRACON Structures and Materials Journal
Revista IBRACON de Estruturas e Materiais
ISSN 1983-4195 ismj.org

ORIGINAL ARTICLE

Flexural and direct tensile strength ratio for concrete unusual cross-sections

Relação entre as resistências à tração na flexão e direta para seções transversais não usuais de concreto

José Anchiêta Damasceno Fernandes Neto[a]
Vladimir Guilherme Haach[a]

[a]Universidade de São Paulo – USP, Escola de Engenharia de São Carlos, Departamento de Engenharia de Estruturas, São Carlos, SP, Brasil

Received 28 April 2021
Accepted 10 March 2022

Abstract: The relationship between flexural and direct tensile strength (α_{fl} ratio) has been explored in evaluations of the cracking moment for concrete structural elements. However, most results for α_{fl} can be applied only for rectangular cross-sections. This manuscript addresses its obtaining for unusual cross-sections largely used in precast concrete elements. A theoretical analysis was performed in thirty-two different cross-sections regarding the compressive strength of concrete and the aggregate type used in the concrete composition. The results showed a smooth increase in α_{fl} for higher strength concretes and lower elastic modulus aggregates. The theoretical procedure showed a good correlation with experimental data and prediction models and can be an interesting alternative for the obtaining of the α_{fl} of unusual cross-sections.

Keywords: flexural tensile strength, direct tensile strength, cracking moment, precast concrete, theoretical analysis.

Resumo: A relação entre a resistência à tração na flexão e tração direta (razão α_{fl}) tem sido explorada na avaliação do momento de fissuração para elementos estruturais de concreto. No entanto, a maioria dos resultados relatados para α_{fl} podem ser aplicados apenas para seções transversais retangulares. Este artigo aborda a obtenção da relação α_{fl} para seções transversais não usuais amplamente utilizadas em elementos de concreto pré-moldado. Uma análise teórica foi realizada em trinta e duas diferentes seções transversais em termos da resistência à compressão do concreto e o tipo de agregado utilizado na composição do concreto. Os resultados apresentaram um suave aumento em α_{fl} para concretos de maior resistência e agregados com menor módulo de elasticidade. O procedimento teórico exibiu uma boa correlação com dados experimentais e modelos de previsão, e pode ser uma alternativa interessante para a obtenção da relação α_{fl} de seções transversais não usuais.

Palavras-chave: resistência à tração na flexão, resistência à tração direta, momento de fissuração, concreto pré-moldado, análise teórica.

How to cite: J. A. D. Fernandes Neto, and V. G. Haach, "Flexural and axial tensile strength ratio for precast concrete structures," *Rev. IBRACON Estrut. Mater.*, vol. 16, no. 1, 16104, 2023, https://doi.org/10.1590/S1983-41952023000100004

1 INTRODUCTION

Concrete is a material of quasi-brittle behavior evaluated predominantly in compression due to its high compressive strength and limited tensile strength. Such low tensile strength property is, therefore, neglected in the design of reinforced concrete structures, and steel reinforcement is used to support tensile stresses [1]. On the other hand, the tensile strength of concrete is an important property in assessments of both cracking formation and deflections at the

Corresponding author: José Anchiêta Damasceno Fernandes Neto.E-mail: anchietafernandes@usp.br
Financial support: Coordenação de Aperfeiçoamento de Pessoal de Nível Superior – Brasil (CAPES) – Finance Code 001 and Conselho Nacional de Desenvolvimento Científico e Tecnológico (Processo 302479/2017-1).
Conflict of interest: Nothing to declare.
Data Availability: The data that support the findings of this study are available from the corresponding author, J. A. D. Fernandes Neto, upon reasonable request.

serviceability limit state [2], and cracking moment in prestressed elements, punching shear, concrete/steel bond strength, shrinkage, control of crack width in early-ages, and development of moment-curvature diagrams [3]. It can be obtained by three different test methods, namely direct tensile test, splitting tensile test, and flexural test.

Splitting and flexural tensile strengths have been widely used and defined from the indirect application of tensile stresses according to EN 12390-6 [4] and EN 12390-5 [5], respectively. However, studies on the determination of the direct tensile strength are limited, since this property is susceptible to testing techniques, such as boundary conditions, loading ratio, and size and shape of the specimens tested [6], [7]. According to Chen et al. [8], although uniaxial tensile tests are challenging, their results are easily interpreted. Contrarily, flexural tests show a nonuniform stress-strain distribution in the cross-section of the specimen, thus hampering the analysis of results. Both tensile strengths (direct, splitting, and flexural) are usually correlated by some standard codes. Although the direct tensile strength is the true tensile strength of concrete, the splitting tensile strength is useful and reliable to estimate the conventional strength due to its simplicity execution. On the other hand, flexural tensile strength can be used to obtain the tensile strength in structural elements subjected to bending. For example, the ABNT NBR 6118 [9] indicates values for the correlation between flexural and direct tensile strength to be used on the verification of the cracking moment for rectangular, I-, T- and inverted T sections.

In general, the direct tensile strength is acquired through correlations between other properties. Figure 1a displays the difference between the tensile behavior for both direct tensile and flexural tests. Direct tensile tests exhibit a linear hardening up to the direct tensile strength (f_{ct}) when a brittle failure occurs. Unlike direct tensile tests, flexural tests show nonlinear hardening after the tensile strength of concrete has been reached and a smooth failure when the flexural tensile strength ($f_{ct,fl}$) has been achieved (see Figure 1a). A typical nonlinear flexural behavior of plain concrete is shown by a moment-curvature relationship (see Figure 1b). Hillerborg et al. [10] proposed a plain concrete behavior under tensile loading based on a fictitious crack model, which considers the presence of a fracture process zone when the maximum stress reaches the tensile strength of concrete (Figures 1c-1d). Such a zone is characterized by a gradual softening of concrete due to micro-cracking and interlocking of the aggregates, cement, or fibers [11], [12]. A fictitious crack is formed in this region simultaneously with a tensile stress decrease in the bottom fiber. When the tensile stress is assumed zero, a real crack is installed, and its width increases according to the softening stress-strain relationship [13] (Figures 1d-1e).

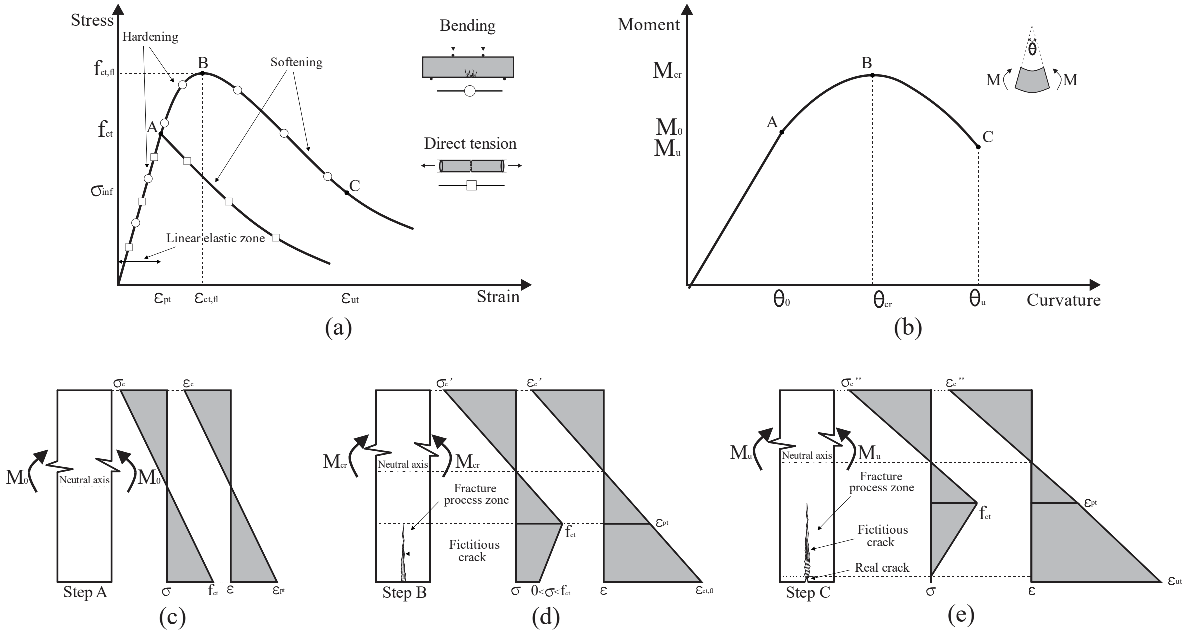

Figure 1. Plain concrete behavior under tensile loading: (a) stress-strain relationship, (b) moment-curvature relationship, and (c-e) stress-strain distribution diagrams along the uncracked and cracked sections.

Flexural tensile strength is essential for evaluations of the cracking moment of concrete elements (Equation 1). In particular, ABNT NBR 6118 [9] recommends the cracking moment verification by Equation 2 with a relationship between flexural and direct tensile strengths, shown in Equation 3:

$$M_{cr} = \frac{f_{ct,fl} \cdot I_g}{y_t} \tag{1}$$

$$M_{cr} = \frac{\alpha_{fl} \cdot f_{ct} \cdot I_g}{y_t} \tag{2}$$

$$\alpha_{fl} = \frac{f_{ct,fl}}{f_{ct}} \tag{3}$$

where M_{cr} is the cracking moment, $f_{ct,fl}$ is the flexural tensile strength, f_{ct} is the direct tensile strength, I_g is the moment of inertia of the gross concrete section, y_t is the distance from the centroidal axis of the gross section, and α_{fl} is the flexural and direct tensile strength ratio.

Some researchers have addressed the flexural and direct tensile strength ratio (α_{fl}) due to differences between the flexural and direct tensile behaviors of concrete and the significance of their correlation. Maalej and Li [13] developed an analytical model to evaluate the flexural strength of fiber cementitious composites and observed the flexural and direct tensile strength ratio depends on the brittleness ratio and is affected by stress distribution in the fracture process zone. Ratio α_{fl} is a function of the specimen geometry and should decrease as the specimen height increases [13], [14]. Sorelli et al. [15] performed bending and uniaxial tensile tests in hybrid fiber-reinforced concretes, and the results indicated both type and fiber geometry highly influence their post-cracking behavior. α_{fl} was 1.46 for plain concrete and increased to 1.86 for macro fiber reinforced concrete.

Wu et al. [6] and Chen et al. [8] studied the effects of strain rate and testing method on the tensile strength of concrete and experimentally compared three methods, namely direct tensile, splitting tensile, and flexural tests for measuring it. The results confirmed the specimens tested under flexure showed higher tensile strength than those subjected to direct and splitting tension. The authors concluded the tensile strength increases and α_{fl} decreases with a strain rate increment, reaching 2.1 to 2.5 values for plain concrete of 37 MPa compressive strength [6], [8]. Balbo [16] evaluated a relationship between splitting tensile strength and flexural strength for dry and plastic concretes used in pavements bases. The experimental data showed the flexural strength is usually 92% and 49% higher than the splitting tensile strength of dry and plastic concretes, respectively. Lin et al. [17] proposed a testing method with embedded steel bars that was considered suitable for assessing the direct tensile strength of normal strength concrete specimens. The results were approximately 50% lower than the flexural tensile strength. α_{fl} varied between 1.92 and 2.02 in tensile tests performed in Ultra-High Performance Fiber Reinforced Cementitious Composites [18].

The studies addressed are limited and report results only for rectangular cross-sections. On the other hand, structural elements with unusual cross-sections have been largely used in several precast concrete industries due to their versatility, production speed, durability, and safety [19]. Besides, such studies usually disregard the influence of strength and aggregate type of the concrete, which are important factors in tensile behavior [20], [21].

This paper evaluates the flexural and direct tensile strength ratio for unusual cross-sections used mainly in precast concrete elements. A theoretical analysis was performed in thirty-two different cross-sections regarding the compressive strength of concrete and the aggregate type used in the mixture. A discussion on the influence of ultimate tensile strain and a comparison between prediction models are also addressed.

2 ANALYTICAL SOLUTION

Ananthan et al. [22] investigated the fracture behavior of plain concrete slender beams subjected to flexural loading using equilibrium equations, and proposed a one-dimensional model, called softening beam model, which accurately predicts the maximum load of rectangular concrete specimens under bending. The model was developed from uncracked ligament equilibrium and use of the strain softening modulus, calculated by Equation 4:

$$E_T = \frac{f_{ct}}{\varepsilon_{ut} - \varepsilon_{pt}} \tag{4}$$

where E_T is the strain softening modulus (MPa), and ε_{ut} and ε_{pt} are the ultimate and peak strains of concrete in tension, respectively.

The relationship between strain softening modulus and elastic modulus is given by

$$E^* = \frac{E_T}{E} \tag{5}$$

where E* is the relation between strain softening modulus and initial modulus and E is the elastic modulus of concrete (MPa).

According to Ananthan et al. [22], ratio E* features the failure mechanism in concrete specimens through the slope of the post-peak softening branch of the tensile stress-strain diagram. The material displays a perfectly brittle behavior when $E^* = \infty$ and perfectly ductile behavior for $E^* = 0$ (see Figure 2a). Figures 2b and 2c show the stress distribution for both perfectly brittle and perfectly ductile behaviors, respectively. The ultimate moment capacity can be obtained from the moment equilibrium of cross-section for both cases, and α_{fl} assumes values of 1.0 and 3.0 for brittle and ductile materials, respectively. Such results indicate the limit range where α_{fl} can be considered [22], [23].

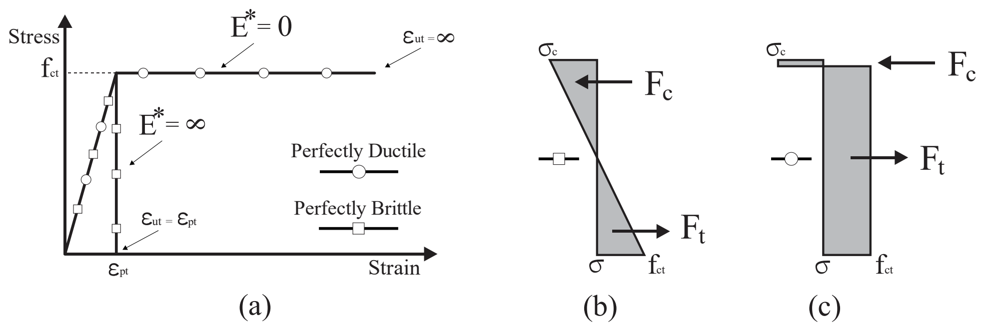

Figure 2. (a) Idealized stress-strain relationship in tension and stress distribution diagrams for (b) perfectly brittle material and (c) perfectly ductile material.

Since a strain softening in tension characterizes the concrete, the idealized stress-strain relationships (Figure 2a) do not apply to an uncracked-ligament real behavior, whose description considers a slope of strain-softening modulus with $0 < E^* < \infty$ (Figure 3a). The softening beam model assumes the stress-strain relationship of concrete in tension can be indicated by a bilinear diagram (Figure 3a). The plane section remains plane after deformation, and the compression behavior simulated is linearly proportional. The equilibrium conditions should be satisfied up to the fracture onset, represented in the stress-strain distribution diagrams in Figure 3b [22].

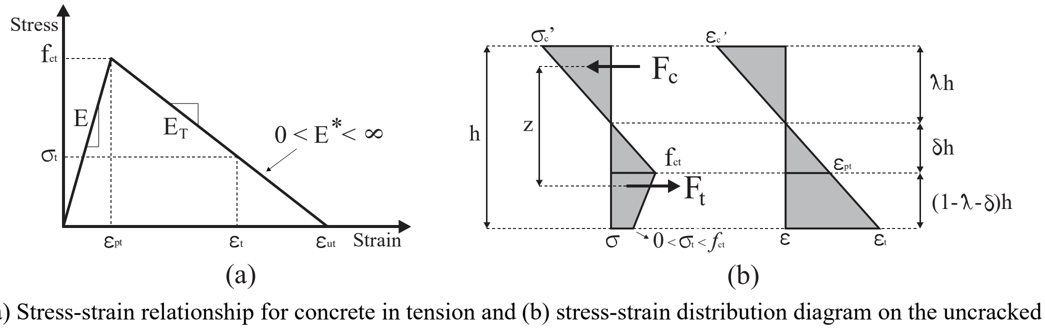

Figure 3. (a) Stress-strain relationship for concrete in tension and (b) stress-strain distribution diagram on the uncracked ligament.

According to the stress-strain relationship in Figure 3a, the stress in the post-peak softening branch is given by

$$\sigma_t = f_{ct} - E_T(\varepsilon_t - \varepsilon_{pt}) \quad (6)$$

where σ_t is the tensile stress (MPa), and ε_t is the corresponding tensile strain.

ε_t can be obtained by Equation 7, derived from the relationships depicted in Figure 3b.

$$\varepsilon_t = \left(\frac{1 - \lambda}{\delta}\right)\varepsilon_{pt} \quad (7)$$

where λ and δ are variable factors from 0 to 1 that characterize the stress-strain distribution diagrams.

Substituting Equation 7 in Equation 6 yields

$$\sigma_t = f_{ct} - \frac{E_T\varepsilon_{pt}(1 - \lambda - \delta)}{\delta} \quad (8)$$

Because of the linear hardening of the stress-strain relationship, the peak strain of concrete in tension can be written as

$$\varepsilon_{pt} = \frac{f_{ct}}{E} \quad (9)$$

Replacing Equations 9 and 5 in Equation 8, the tensile stress in softening portion is given by

$$\sigma_t = f_{ct}\left[1 - E^* \frac{(1 - \lambda - \delta)}{\delta}\right] \quad (10)$$

According to the stress distribution diagram (Figure 3b), the compressive stress can be obtained by:

$$\sigma_c' = f_{ct} \cdot \frac{\lambda}{\delta} \quad (11)$$

where σ_c' is the compressive stress (MPa).

The compressive and tensile horizontal forces acting on the uncracked ligament (Equations 12 and 13, respectively) are defined multiplying the tensile strength of concrete by the area of the stress distribution diagram:

$$F_c = \frac{\sigma_c' \cdot \lambda \cdot h \cdot b_w}{2} \quad (12)$$

$$F_t = \frac{f_{ct} \cdot \delta \cdot h \cdot b_w}{2} + \frac{(f_{ct} + \sigma_t)}{2}(1 - \lambda - \delta) \cdot h \cdot b_w \quad (13)$$

where F_c is the horizontal compressive force (N), F_t is the horizontal tensile force (N), h is the rectangular section height (mm), and b_w is a rectangular section width (mm).

The first equilibrium condition should be satisfied, since no external horizontal forces act on the section, thus:

$$F_c + F_t = 0 \tag{14}$$

$$\frac{1}{2}\left(\sigma_c{}' \cdot \lambda \cdot h \cdot b_w\right) = \frac{1}{2}\left(f_{ct} \cdot \delta \cdot h \cdot b_w\right) + \frac{1}{2}(f_{ct} + \sigma_t)(1 - \lambda - \delta) \cdot h \cdot b_w \tag{15}$$

Substituting Equations 10 and 11 in Equation 15, the first equilibrium condition is defined as

$$\lambda^2\left(1 + E^*\right) + 2\lambda\left(\delta + E^*\delta - E^*\right) + \left[\delta^2\left(1 + E^*\right) - 2\delta\left(1 + E^*\right) + E^*\right] = 0 \tag{16}$$

The solution to the quadratic equation is given by

$$\lambda = \frac{-\left(\delta + E^*\delta - E^*\right) \pm \sqrt{2E^*\delta + 2\delta - E^*}}{\left(1 + E^*\right)} \tag{17}$$

The moment equilibrium condition is accepted when the external bending moment is equal to the ultimate moment capacity generated by the horizontal tensile force on the compression center, and can be written as

$$M_{cr} = \frac{b_w \cdot h^2}{6}\left[2f_{ct} \cdot \delta\left(\lambda + \delta\right) + \sigma_t\left(1 - \lambda - \delta\right)\left(\lambda + 3\delta + 3\right) + (f_{ct} - \sigma_t)(1 - \lambda - \delta)\left(\lambda + 2\delta + 1\right)\right] \tag{18}$$

Finally, applying properties I_g and y_t for rectangular cross-section, and replacing Equation 18 in Equation 2, Ananthan et al. [22] defined α_{fl} as

$$\alpha_{fl} = 3 - 2\lambda + E^* \frac{\left(\delta + 2\right)}{\delta}\left(2\delta + 2\lambda - 1\right) - \left(\delta + \lambda\right)^2\left[1 + \frac{E^*\left(\delta + 2\right)}{\delta}\right] \tag{19}$$

Equation 19 represents α_{fl} for a rectangular cross-section. It is noteworthy that the characterization of the stress distribution diagram and knowledge of the stress-strain relationship in tension are sufficient to obtain α_{fl}.

3 SOLUTION FOR UNUSUAL CROSS-SECTIONS

The theoretical analysis was developed in two phases. The first involved the definition of the geometry of the cross-sections and mechanical parameters employed, whereas in the second, the ultimate moment capacity of the cross-sections was calculated by the moment-curvature diagram, and α_{fl} was obtained for normal and high strength concretes of 20 to 90 MPa. Six different aggregate types, namely basalt, diabase, granite, gneiss, limestone, and sandstone were considered in each series.

3.1 Geometry of the cross-sections of precast concrete structures

Thirty-two cross-sections usually applied in precast concrete structures were employed. They were divided into four groups of eight and coined according to both structural element type and application position in situ. The BCS Group was comprised of one-dimensional structural elements frequently used in precast concrete buildings, such as beams, columns, and piles, and the FLS Group considered structural elements of one and two dimensions employed in buildings and bridge floors (e.g., slabs, rails, filler blocks, and double tees). Structural elements, such as U and Y-beams and tiles used in roofs of commercial and industrial buildings were inserted in the RFS group. Finally, the BRS Group was comprised of buried large structural elements employed in waterway and highway infrastructures (e.g., culverts and tunnels). Figure 4 illustrates the geometry of the cross-sections evaluated.

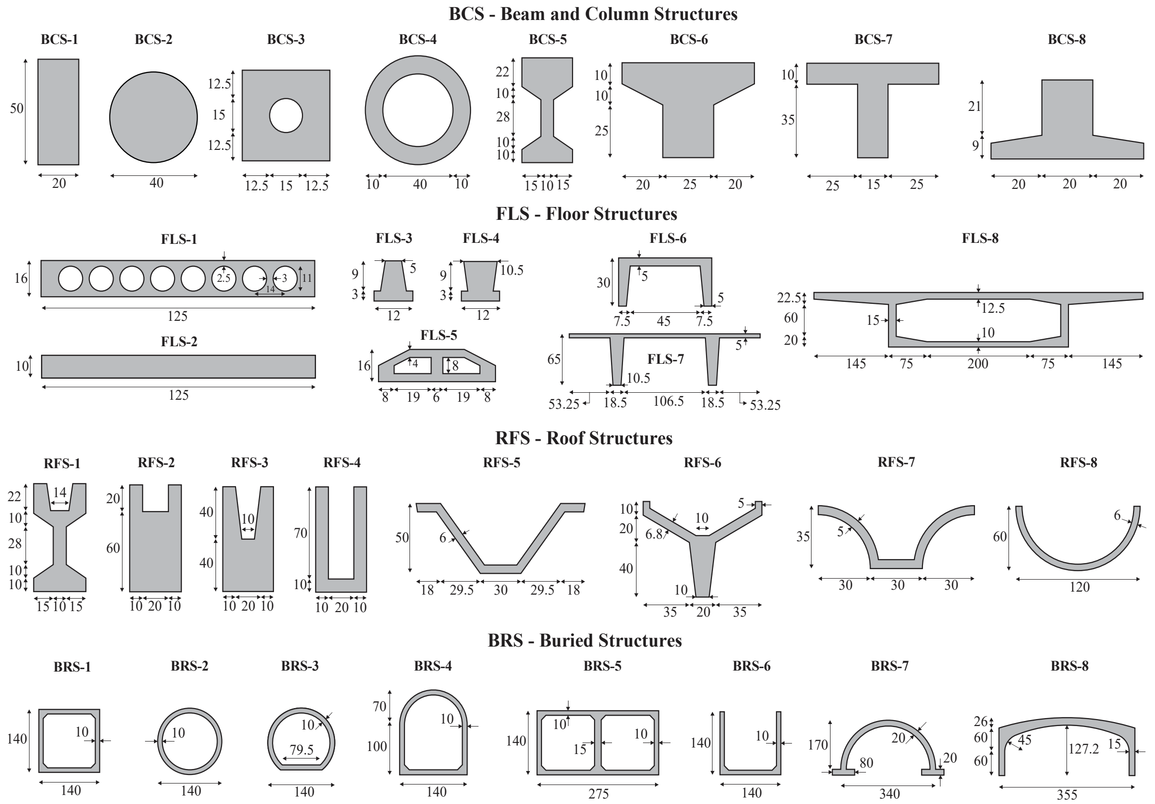

Figure 4. Geometry of the cross-sections of precast concrete groups (dimensions in cm).

3.2 Mechanical parameters

The compressive behavior of concrete was described from a parabola-rectangle stress-strain relationship recommended by ABNT NBR 6118 [9], which shows an initial parabolic branch, and a constant branch between the strain at the maximum compressive strength and the ultimate compressive strain. [9]. The tensile behavior of concrete is represented by a bilinear stress-strain relationship proposed by Bažant and Oh [24]. This law considers a linear hardening characterized by the elastic modulus, and a linear softening after the tensile strength of concrete has been reached. Its ultimate tensile strain was 10 times greater than the peak tensile strain ($\varepsilon_{ut} = 10\varepsilon_{pt}$) according to ACI 224.2R [25]. Safety factors β and γ_c were considered in stress-strain diagrams and assumed values of 0.85 and 1.4, respectively, in accordance with ABNT NBR 6118 [9]. In this paper, the steel reinforcement contribution was not considered because only the portion of tensile strength of concrete is employed to assess the cracking moment of the structural elements. Figure 5 shows the compressive and tensile behaviors of concrete.

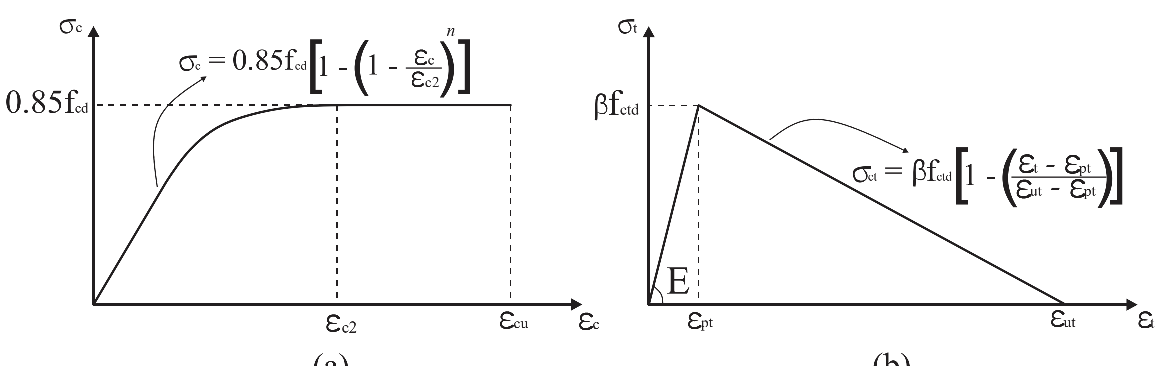

Figure 5. Mechanical behavior of concrete: (a) Compression and (b) tension.

The mechanical properties were obtained from the characteristic compressive strength of concrete (f_{ck}) using relationships indicated in ABNT NBR 6118 [9], leading to valid results. Table 1 displays the relationships employed for the mechanical properties of concrete.

Table 1. Summary of the mechanical properties of concrete.

Property	$f_{ck} \leq 50$ MPa	$f_{ck} > 50$ MPa
f_{cd}	f_{ck}/γ_c	f_{ck}/γ_c
f_{ctd}	$0.21 f_{ck}^{2/3}/\gamma_c$	$0.7\left[2.12\ln\left(1+0.11f_{ck}\right)\right]/\gamma_c$
E	$5600\alpha_e f_{ck}^{1/2}$	$21500\alpha_e\left(0.1f_{ck}+1.25\right)^{1/3}$
ε_{c2}	2.0‰	$2.0‰ + 0.085‰\left(f_{ck}-50\right)^{0.53}$
ε_{cu}	3.5‰	$2.6‰ + 35‰\left[\left(90-f_{ck}\right)/100\right]^{4}$
n	2.0	$1.4 + 23.4\left[\left(90-f_{ck}\right)/100\right]^{4}$
ε_{pt}	$\beta f_{ctd}/E$	$\beta f_{ctd}/E$
ε_{ut}	$10\varepsilon_{pt}$	$10\varepsilon_{pt}$

Note: f_{ck} is the characteristic compressive strength of concrete (MPa), f_{cd} is the design compressive strength of concrete (MPa), f_{ctd} is the design tensile strength of concrete (MPa), E is the elastic modulus of concrete (MPa), α_e is the correction factor of elastic modulus according to aggregate type, ε_{c2} is the strain at the maximum compressive strength, ε_{cu} is the ultimate compressive strain, ε_{ut} is the ultimate tensile strain, ε_{pt} is the peak tensile strain, n is the exponent of compressive stress law, and β and γ_c are safety factors.

The ultimate moment capacity was determined by the moment-curvature relations from a section analysis of the precast concrete elements. The geometry of the cross-sections, mechanical properties, stress-strain diagrams of concrete, force equilibrium, and strain compatibility were used for the obtaining of the moment-curvature relationships, assuming plane sections remained plane after bending. The neutral axis depth was adjusted for a given compressive strain of concrete, for satisfying the equilibrium of the internal forces, and the moment was calculated. The moment-curvature curves exhibited a linear branch up to the peak tensile strain of concrete, with a subsequent nonlinear behavior until the ultimate tensile strain had been achieved. The elastic modulus was multiplied by a correction factor (α_e) that assumed values of 1.2, 1.0, 0.9 and 0.7 for mix compositions with basalt/diabase, granite/gneiss, limestone and sandstone, respectively, for consideration of the different aggregate types, thus changing the peak and ultimate tensile strain of concrete. Finally, Equation 20 determined α_{fl}.

$$\alpha_{fl} = \frac{M_{cr} \cdot y_t}{\beta \cdot f_{ctd} \cdot I_g} \tag{20}$$

4 RESULTS AND DISCUSSIONS

Firstly, the theoretical model was compared with a combination of experimental results from flexural and uniaxial tensile tests conducted by Sorelli et al. [15], Lin et al. [17] and Wee et al. [26] in rectangular cross-section specimens. Different samples were tested under direct tensile and four- or three-point bending. The tensile strength of concrete was evaluated in models with 3 to 90-day curing time and 10 to 70 MPa compressive strength for distinct mix compositions.

The experimental and theoretical results of the comparison of α_{fl} (Figure 6) show the theoretical model reasonably agreed with the experimental data. The higher differences were observed in tests performed at early ages, which showed small compressive strength. Numerous operations are performed on the specimens at this stage, and their properties are widely influenced by temperature, humidity, and curing conditions [1]. Besides, the drying shrinkage occurs by the imposition of tensile stress fields on concrete [16]. The difference between experimental and theoretical results was approximately 10%, considering normal and high strength concretes above 20 MPa. Therefore, the theoretical model showed a good fit for the strengths scope considered in this study.

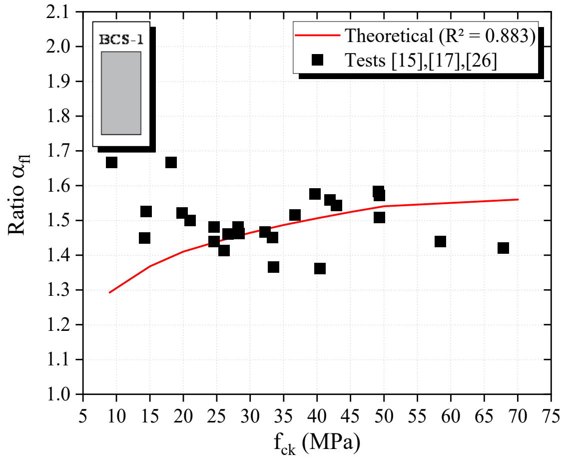

Figure 6. Comparison between theoretical and experimental results.

The results were also divided into two topics. Firstly, α_{fl} was addressed in terms of compressive strength of concrete, aggregate type used in the mixture, and ultimate tensile strain, and in the second topic, it was compared according to different prediction models.

4.1 Influence of compressive strength of concrete and aggregate type

An extensive theoretical analysis evaluated the influence of the compressive strength of concrete and aggregate type on α_{fl}. Table 2 shows α_{fl} calculated for a typical concrete with f_{ck} = 40 MPa and different types of aggregates. The results indicate the aggregate type used in the mix composition exerts a moderate influence on α_{fl}. Low-stiffness aggregates provided greater deformability to the concrete [27], and compositions obtained higher values for α_{fl}. The use of basaltic aggregates as reference promoted up to 12.9%, 6.9% and 4.3% increases for concretes that used sandstone, limestone, and granite aggregates, respectively, for all series analyzed. The difference decreased in function of the increase in the compressive strength of concrete.

Table 2. Variation in α_{fl} according to aggregate type for f_{ck} = 40 MPa.

Group	Section	Aggregate type				Mean	CV (%)
		Basalt or Diabase	Granite or Gneiss	Limestone	Sandstone		
BCS	BCS-1	1.46	1.51	1.54	1.61	1.53	4.10
	BCS-2	1.68	1.75	1.79	1.87	1.77	4.48
	BCS-3	1.40	1.45	1.46	1.52	1.46	3.38
	BCS-4	1.43	1.46	1.50	1.54	1.48	3.23
	BCS-5	1.19	1.22	1.23	1.26	1.23	2.36
	BCS-6	1.40	1.44	1.47	1.52	1.46	3.47
	BCS-7	1.38	1.41	1.42	1.46	1.42	2.33
	BCS-8	1.37	1.41	1.43	1.49	1.43	3.51
FLS	FLS-1	1.26	1.29	1.31	1.33	1.30	2.30
	FLS-2	1.46	1.51	1.54	1.61	1.53	4.10
	FLS-3	1.40	1.45	1.48	1.55	1.47	4.27
	FLS-4	1.38	1.42	1.45	1.51	1.44	3.80
	FLS-5	1.32	1.35	1.37	1.42	1.37	3.08
	FLS-6	1.42	1.46	1.47	1.51	1.47	2.52
	FLS-7	1.44	1.48	1.49	1.53	1.49	2.49
	FLS-8	1.08	1.09	1.10	1.12	1.10	1.56
RFS	RFS-1	1.22	1.24	1.26	1.29	1.25	2.38
	RFS-2	1.48	1.54	1.57	1.66	1.56	4.80

Table 2. Continued...

Group	Section	Aggregate type				Mean	CV (%)
		Basalt or Diabase	Granite or Gneiss	Limestone	Sandstone		
	RFS-3	1.51	1.57	1.60	1.68	1.59	4.45
	RFS-4	1.31	1.35	1.38	1.44	1.37	4.00
	RFS-5	1.27	1.31	1.33	1.38	1.32	3.46
	RFS-6	1.53	1.59	1.62	1.70	1.61	4.39
	RFS-7	1.23	1.26	1.27	1.32	1.27	2.95
	RFS-8	1.37	1.42	1.44	1.51	1.44	4.04
BRS	BRS-1	1.12	1.14	1.16	1.19	1.15	2.59
	BRS-2	1.29	1.32	1.34	1.39	1.34	3.15
	BRS-3	1.17	1.21	1.22	1.26	1.22	3.04
	BRS-4	1.13	1.16	1.18	1.22	1.17	3.22
	BRS-5	1.11	1.13	1.14	1.18	1.14	2.58
	BRS-6	1.14	1.17	1.19	1.24	1.19	3.55
	BRS-7	1.18	1.21	1.23	1.27	1.22	3.09
	BRS-8	1.40	1.44	1.46	1.51	1.45	3.15

Figure 7 more clearly shows the influence of the aggregate type on α_{fl}. According to the correlations between the mechanical properties of concrete in Table 1, the elastic modulus reduction due to the aggregate type caused more deformability and improved the ultimate tensile strain of the concrete. Additionally, for the same tensile strength of concrete, the increase in the ultimate tensile strain reduced the softening branch slope and the strain softening modulus (E_T), increasing α_{fl}. On the other hand, the α_{fl} ratio of concretes with aggregates of lower elastic modulus showed a smaller increment than concretes with aggregates of larger elastic modulus (Figure 7). α_{fl} can be sequentially higher in concretes with basalt, granite, limestone and sandstone, respectively, for the same ultimate tensile strain value.

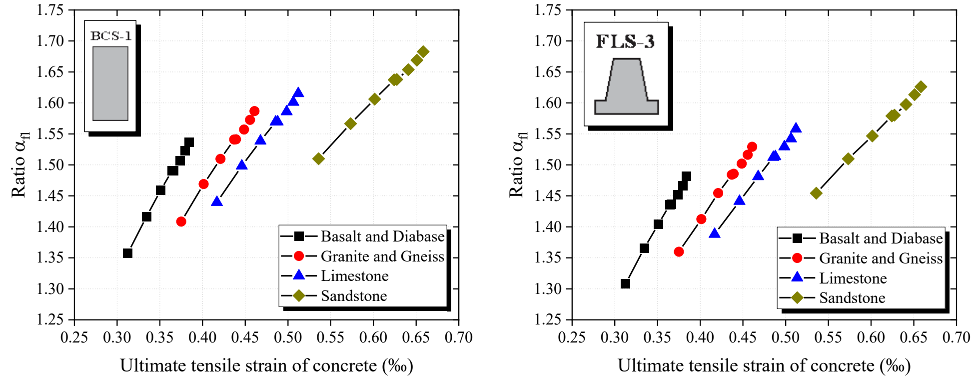

Figure 7. Variation in α_{fl} with ultimate tensile strain for BCS-1 and FLS-3.

The increase in the compressive strength of concrete conduct to an increase in the tensile strength of the concrete reducing the neutral axis depth (λ) in structural elements subjected to bending (see Figure 4b), which smoothly increases the α_{fl} ratio, according to Equation 19. The α_{fl} value increased to 9.5% on average when the compressive strength of concrete improved from 20 MPa to 90 MPa. However, normal strength concretes (20 MPa to 50 MPa) showed an up to 7% increase against only 2.5% of high strength ones (60 MPa to 90 MPa).

Figures 8, 9, 10 and 11 show α_{fl} in terms of compressive strength of concrete and aggregate type for BCS, FLS, RFS and BRS groups, respectively.

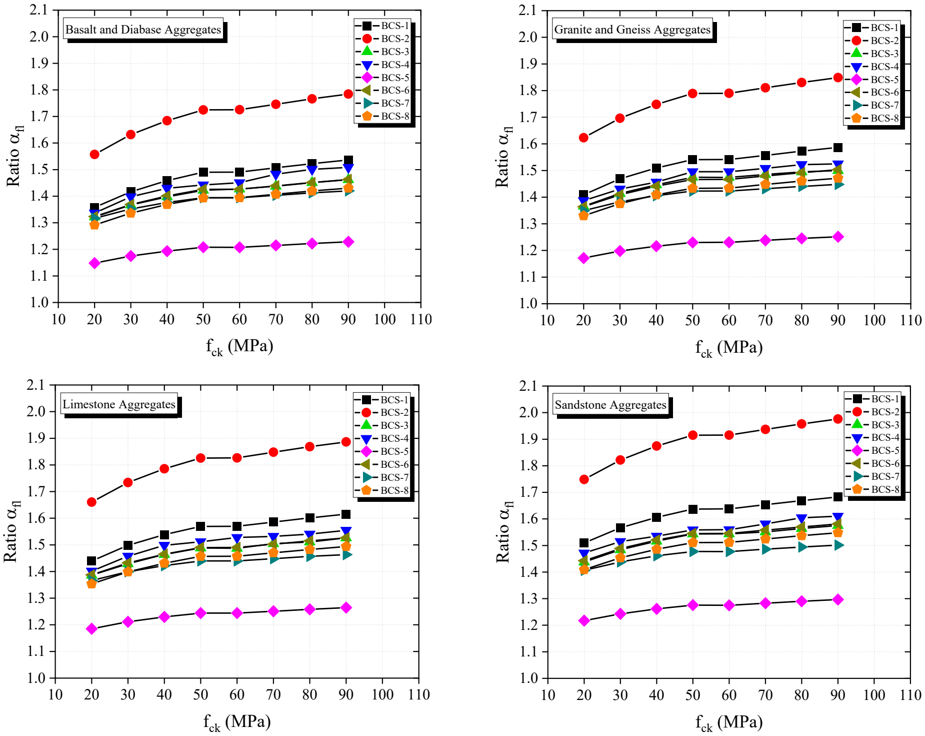

Figure 8. Variation in α_{fl} with compressive strength for BCS Group.

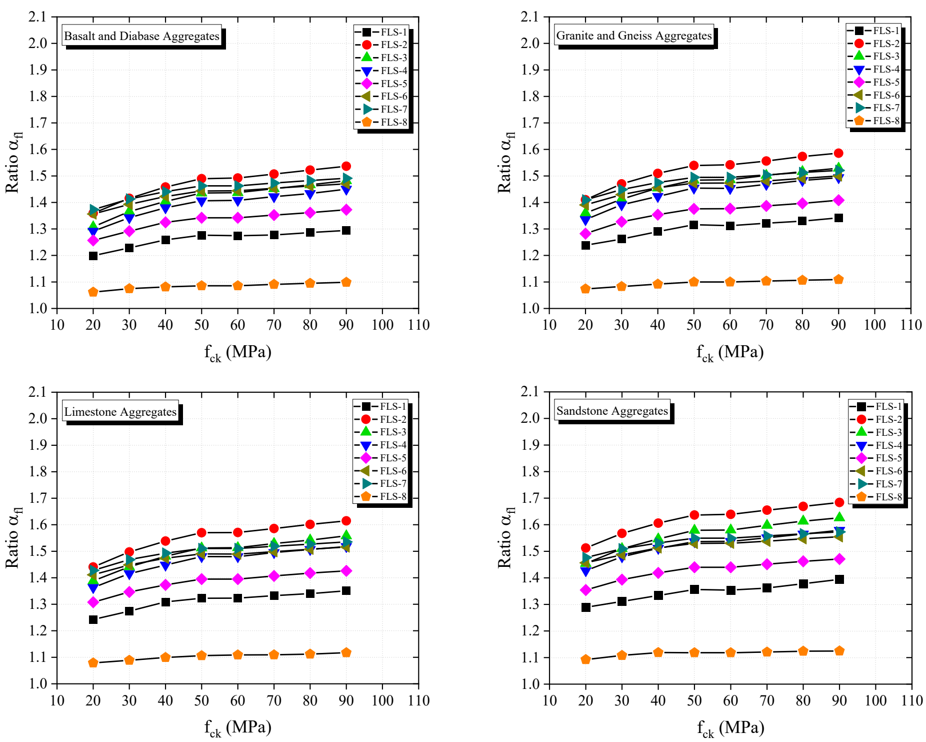

Figure 9. Variation in α_{fl} with compressive strength for FLS Group.

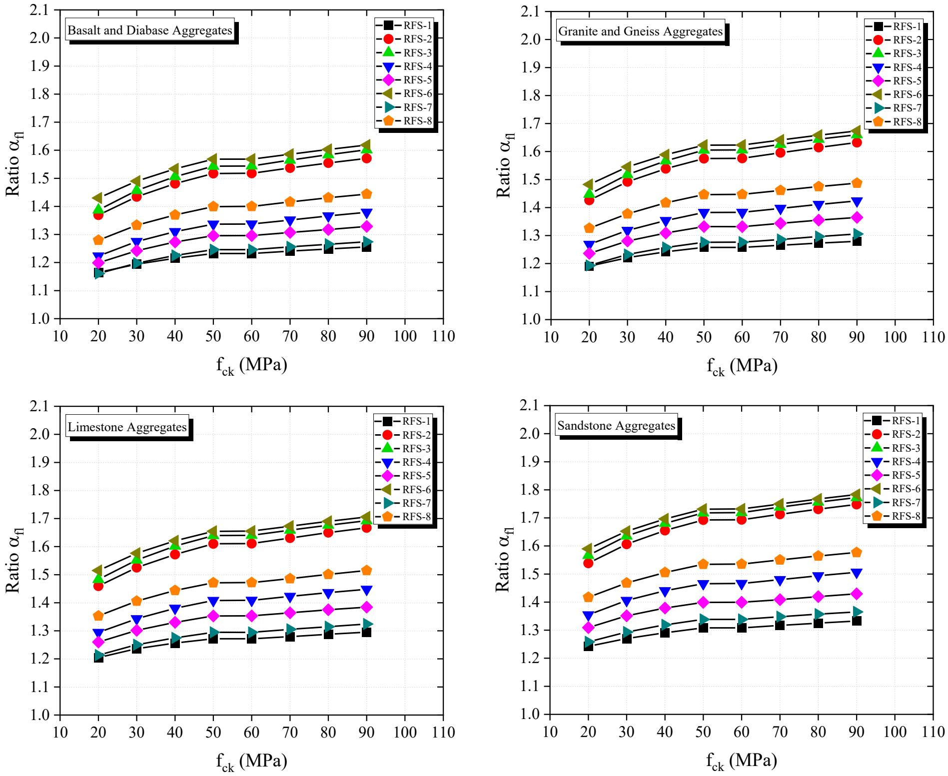

Figure 10. Variation in α_{fl} with compressive strength for RFS Group.

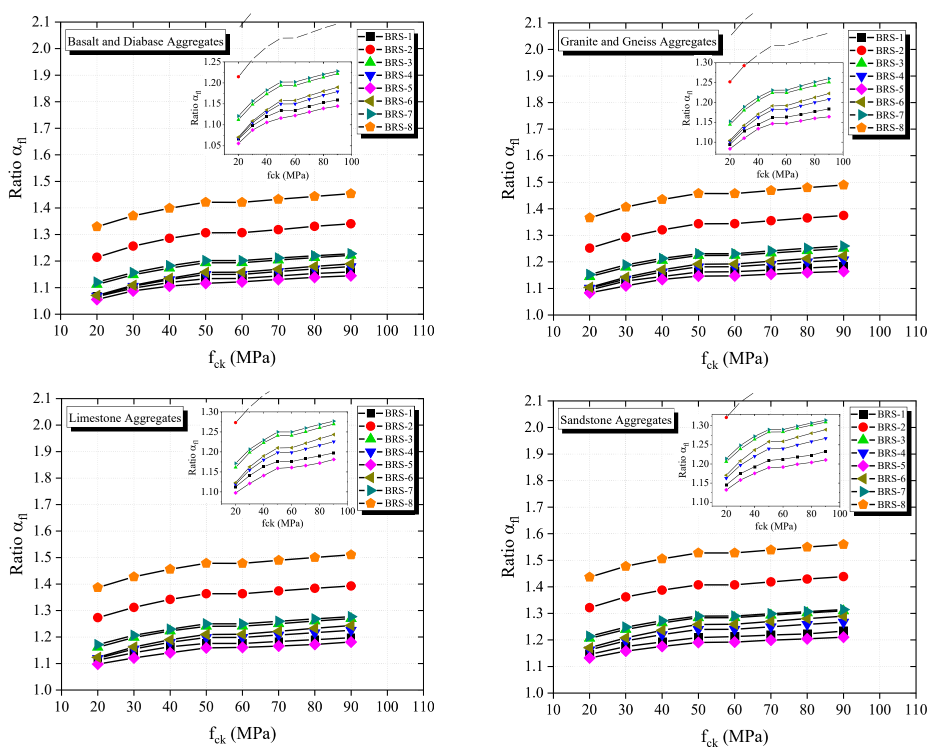

Figure 11. Variation in α_{fl} with compressive strength for BRS Group.

The α_{fl} variation in terms of compressive strength of concrete showed constant values for 50 MPa and 60 MPa compressive strengths due to the distinct mechanical parameters adopted for normal and high strength concretes (Table 1). Regarding mechanical properties, the linear compressive stress-strain relationship employed in the analytical solution proposed by Ananthan et al. [22] was different from the parabola-rectangle stress-strain one used in this study. However, the ultimate moment capacity produces small compressive stresses in the top fiber of the cross-section, and the stress-strain relationship in compression exerts a small influence on α_{fl}.

According to the results, 75.1% of the calculated values of α_{fl} remained between 1.20 and 1.60. Values above this range were mostly obtained by circular cross-section (BCS-2), rectangular cross-sections (BCS-1 and FLS-2), and U and Y-beams (RFS-2/3/6) used as roof structural elements. On the other hand, 14.6% of the results ($\alpha_{fl} < 1.20$) were associated with large structural elements, such as cross-sections for box culverts (BRS-1/3/4/5) and box girder bridges (FLS-8). The α_{fl} decrease in such structural elements may be related to the size effect phenomenon. According to [28]-[30], the flexural tensile strength of specimens of large dimensions is reduced due to an increase in the cross-section height. In this study, the size effect was milder in elements with circular segments, such as cross-sections for tunnels (BRS-2/7/8).

4.2 Comparison with prediction models

The theoretical results of α_{fl} were compared with different prediction models from the literature. Codes for the design of concrete structures have shown fixed values or simple expressions for α_{fl}. According to Model Code [14], α_{fl} depends only on the cross-section height and is reduced with its increase. In contrast, ABNT NBR 6118 [9] recommends the use of fixed values for α_{fl}. Both models disregard the mechanical characteristics of the structural element.

Based on nonlinear fracture mechanics, Buchaim [23], Müller and Hilsdorf [31] and Rokugo et al. [32] proposed analytical models considering the influence of the characteristic length (l_{ch}) on the flexural behavior, defined by Hillerborg et al. [10] according to both fracture energy and mechanical properties of concrete. Although this parameter has no direct physical meaning, it is a property that determines the fracture process zone size [13]. Table 3 shows the summarized expressions of the codes and authors for the prediction of α_{fl}.

Table 3. Summary of the expressions for α_{fl}.

Model	Ratio α_{fl}
Model Code [14]	$\alpha_{fl} = \frac{1+0.06h^{0.7}}{0.06h^{0.7}}$
Müller and Hilsdorf [31]	$\alpha_{fl} = \frac{\left[1+\alpha_{mh}\left(0.01h\right)^{0.7}\right]}{\left(\alpha_{mh}\left(0.01h\right)^{0.7}\right)}$; with $\alpha_{mh} = 0.8 + \frac{5}{\left(0.01l_{ch}\right)^{1.5}}$ and $l_{ch} = \frac{G_f E}{f_{ct}^2}$
ABNT NBR 6118 [9]	α_{fl} = 1.5, 1.3 or 1.2 for rectangular, I and T beams, respectively.
Buchaim [23]	$\alpha_{fl} = 1 + 2\eta\left[\frac{3-6\eta+3\left(1-B\right)\eta^2+2B\eta^3}{3-6\eta+\left(B+3\right)\eta^2}\right]$; with $\eta = \frac{a_d}{h}$ and $B = \frac{f_{ct}^2 L}{2G_f E}$
Rokugo et al. [32]	$\alpha_{fl} = \frac{\left[1+0.85+4.5\left(h/l_{ch}\right)\right]}{\left[0.85+4.5\left(h/l_{ch}\right)\right]}$; with $l_{ch} = \frac{G_f E}{f_{ct}^2}$

Note: λ and δ are factors of the characterization of the stress-strain distribution diagram, h is the cross-section height (mm), l_{ch} is the characteristic length (mm), G_f is the fracture energy of concrete (N.mm), E is the elastic modulus of concrete (MPa), f_{ct} is the direct tensile strength of concrete (MPa), a_d is the fictitious crack height (mm), and L is the structural element length (mm).

Figure 12 shows α_{fl} for each prediction model compared to theoretical results for rectangular cross-section (BCS-1). The energy fracture was obtained according to the Model Code [14], and a 0.10 h/L ratio was considered. Predictions of design codes do not compute the concrete composition and show constant values for α_{fl}. The results ranged between 1.22 and 1.50 for Model Code [14] and ABNT NBR 6118 [9], respectively, whereas in the other prediction models, they varied up to 10% due to an increase in the compressive strength of concrete. The largest variations between the prediction models evaluated ranged between 36.8% and 26.5% for normal and high strength concretes, respectively.

Although most prediction models are defined only for rectangular cross-sections, ABNT NBR 6118 [9] establishes α_{fl} for I and T beams – see Figure 13 for a comparison of α_{fl} for rectangular, and I and T beams.

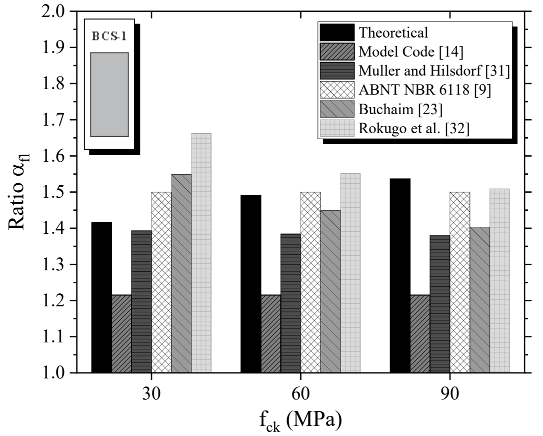

Figure 12. Comparison of α_{fl} obtained by different prediction models.

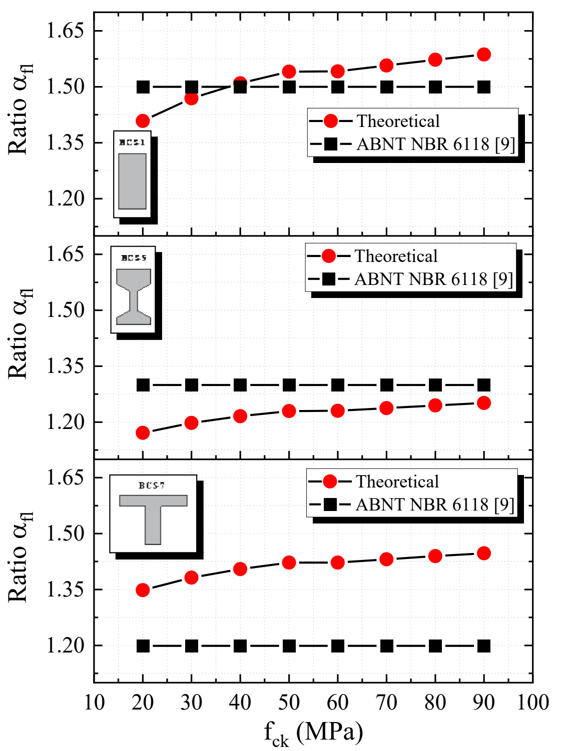

Figure 13. α_{fl} for rectangular, I and T beams: Theoretical results vs. ABNT NBR 6118 [9].

In general, the theoretical procedure used in this study showed a good agreement with the prediction models described, except for Model Code [14], which was more conservative. A greater disparity was observed for low strength concretes, which subsequently balanced α_{fl} with the increase in the compressive strength.

5 CONCLUSIONS

This study reported a theoretical analysis of ratio α_{fl} for unusual cross-sections widely used in precast concrete structures. Thirty-two different cross-sections were evaluated and divided into four groups of elements commonly employed in beams, columns, floors, roofs, and buried structures. Fictitious crack model considerations were used in the theoretical analysis for the obtaining of the ultimate moment capacity of precast concrete elements. Parametric studies investigated the effects of the compressive strength of concrete and aggregate type of the mix composition on α_{fl}. Normal and high strength concretes of 20 MPa to 90 MPa compressive strength and six aggregate types were considered in the analysis.

An increment in the compressive strength of concrete smoothly increased α_{fl}. Similarly, lower elastic modulus aggregates caused a greater deformability in the concrete and increased α_{fl}. Such an increment in α_{fl} due to the compressive strength and aggregate type was higher in normal strength concretes than in high strength ones. The analyses revealed 75.1% of ratio α_{fl} results ranged between 1.20 and 1.60, highlighting its higher values for circular, rectangular, and U and Y beams. On the other hand, buried large cross-sections showed a significant decrement in α_{fl} due to the size effect.

The proposed methodology was compared with experimental results, and prediction models from the literature showed a reasonable agreement, with more significant differences observed concerning the Model Code [14]. According to the results, the theoretical procedure has proven a viable alternative and can be a consistent way for assessing the α_{fl} of precast concrete elements with unusual cross-sections.

ACKNOWLEDGEMENTS

This study was partially financed by the Coordenação de Aperfeiçoamento de Pessoal de Nível Superior – Brasil (CAPES) – Finance Code 001 and CNPq (Brazilian government agency for research - Finance Code Nº 302479/2017-1).

REFERENCES

[1] P. K. Mehta and P. J. M. Monteiro, *Concrete: Microstructure, properties and materials*, 3rd ed. New York, United States: McGraw-Hill, 2006.

[2] American Concrete Institute, *Building code requirements for structural concrete*, ACI Committee 318, 2019.

[3] R. V. Silva, J. de Brito, and R. K. Dhir, "Tensile strength behaviour of recycled aggregate concrete," *Constr. Build. Mater.*, vol. 83, pp. 108–118, May 2015, http://dx.doi.org/10.1016/j.conbuildmat.2015.03.034.

[4] European Committee for Standardization, *Testing hardened concrete: Tensile splitting strength of test specimens*, EN 12390-6, 2009.

[5] European Committee for Standardization, *Testing hardened concrete: Flexural strength of test specimens*, EN 12390-5, 2019.

[6] S. Wu, X. Chen, and J. Zhou, "Tensile strength of concrete under static and intermediate strain rates: Correlated results from different testing methods," *Nucl. Eng. Des.*, vol. 250, pp. 173–183, Sep 2012, http://dx.doi.org/10.1016/j.nucengdes.2012.05.004.

[7] J. Á. López, P. Serna, J. Navarro-Gregori, and E. Camacho, "An inverse analysis method based on deflection to curvature transformation to determine the tensile properties of UHPFRC," *Mater. Struct.*, vol. 48, pp. 3703–3718, Oct 2015, http://dx.doi.org/10.1617/s11527-014-0434-0.

[8] X. Chen, S. Wu, J. Zhou, Y. Chen, and A. Qin, "Effect of testing method and strain rate on stress-strain behavior of concrete," *J. Mater. Civ. Eng.*, vol. 25, no. 11, pp. 1752–1761, Nov 2013, http://dx.doi.org/10.1061/(ASCE)MT.1943-5533.0000732.

[9] Associação Brasileira de Normas Técnicas, *Projeto de estruturas de concreto: Procedimento*, ABNT NBR 6118, 2014.

[10] A. Hillerborg, M. Modéer, and P.-E. Petersson, "Analysis of crack formation and crack growth in concrete by means of fracture mechanics and finite elements," *Cement Concr. Res.*, vol. 6, no. 6, pp. 773–781, Nov 1976. http://dx.doi.org/10.1016/0008-8846(76)90007-7.

[11] A. R. Murthy, B. L. Karihaloo, N. R. Iyer, and B. K. R. Prasad, "Bilinear tension softening diagrams of concrete mixes corresponding to their size-dependent specific fracture energy," *Constr. Build. Mater.*, vol. 47, pp. 1160–1166, Oct 2013., http://dx.doi.org/10.1016/j.conbuildmat.2013.06.004.

[12] M. Maalej and V. C. Li, "Flexural/tensile-strength ratio in engineered cementitious composites," *J. Mater. Civ. Eng.*, vol. 6, no. 4, pp. 513–528, Nov 1994, http://dx.doi.org/10.1061/(ASCE)0899-1561(1994)6:4(513).

[13] M. Maalej and V. C. Li, "Flexural strength of fiber cementitious composites," *J. Mater. Civ. Eng.*, vol. 6, no. 3, pp. 390–406, Nov 1994, http://dx.doi.org/10.1061/(ASCE)0899-1561(1994)6:3(390).

[14] International Federation for Structural Concrete, *fib Model Code 2010*, MC2010, 2010.

[15] L. G. Sorelli, A. Meda, and G. A. Plizzari, "Bending and uniaxial tensile tests on concrete reinforced with hybrid steel fibers," *J. Mater. Civ. Eng.*, vol. 17, no. 5, pp. 519–527, Oct 2005, http://dx.doi.org/10.1061/(ASCE)0899-1561(2005)17:5(519).

[16] J. T. Balbo, "Relations between indirect tensile and flexural strengths for dry and plastic concretes," *Rev. IBRACON Estrut. Mater.*, vol. 6, no. 6, pp. 854–874, Dec 2013, http://dx.doi.org/10.1590/S1983-41952013000600003.

[17] W. T. Lin, A. Cheng, R. Huang, and T. C. Cheng, "A method for testing the strength of concrete using uniaxial direct tension," *J. Chin. Inst. Eng.*, vol. 36, no. 3, pp. 295–303, Jul 2013, http://dx.doi.org/10.1080/02533839.2012.725912.

[18] F. L. Monte and L. Ferrara, "Tensile behaviour identification in Ultra-High Performance Fibre Reinforced Cementitious Composites: indirect tension tests and back analysis of flexural test results," *Mater. Struct.*, vol. 53, no. 145, pp. 1–12, Nov 2020, http://dx.doi.org/10.1617/s11527-020-01576-8.

[19] V. G. Haach and M. A. C. Paiva, "Application of the rebound test for the technological control of concrete hollow-core slabs," *Rev. IBRACON Estrut. Mater.*, vol. 13, no. 4, pp. 1–14, Aug 2020, http://dx.doi.org/10.1590/S1983-41952020000400006.

[20] K. P. Vishalakshi, V. Revathi, and S. S. Reddy, "Effect of type of coarse aggregate on the strength properties and fracture energy of normal and high strength concrete," *Eng. Fract. Mech.*, vol. 194, pp. 52–60, May 2018, http://dx.doi.org/10.1016/j.engfracmech.2018.02.029.

[21] S. J. Choi, K. H. Yang, J. I. Sim, and B. J. Choi, "Direct tensile strength of lightweight concrete with different specimen depths and aggregate sizes," *Constr. Build. Mater.*, vol. 63, pp. 132–141, Jul 2014, http://dx.doi.org/10.1016/j.conbuildmat.2014.04.055.

[22] H. Ananthan, B. K. Raghuprasad, and K. T. Sundara Raja Iyengar, "Influence of strain softening on the fracture of plain concrete beams," *Int. J. Fract.*, vol. 45, pp. 195–219, Sep 1990, http://dx.doi.org/10.1007/BF00693349.

[23] R. Buchaim, "A influência da não-linearidade física do concreto armado na rigidez à flexão e na capacidade de rotação plástica," Ph.D dissertation, Dept. Eng. Estrut. Fund., Univ. São Paulo, São Paulo, 2001.

[24] Z. P. Bažant and B. H. Oh, "Crack band theory for fracture of concrete," *Mater. Struct.*, vol. 16, no. 145, pp. 155–177, May 1983, http://dx.doi.org/10.1007/BF02486267.

[25] American Concrete Institute, *Cracking of concrete members in direct tension*, ACI Committee 224.2R, 1997.

[26] T. H. Wee, H. R. Lu, and S. Swaddiwudhipong, "Tensile strain capacity of concrete under various state of stress," *Mag. Concr. Res.*, vol. 52, no. 3, pp. 185–193, Jun 2000. http://dx.doi.org/10.1680/macr.2000.52.3.185.

[27] R. W. Sun and G. C. Fanourakis, "An assessment of factors affecting the elastic modulus of concrete," *Struct. Concr.*, vol. 22, no. 1, pp. 1–11, Feb 2021. http://dx.doi.org/10.1002/suco.202000553.

[28] A. Carpinteri and G. Ferro, "Size effects on tensile fracture properties: A unified explanation based on disorder and fractality of concrete microstructure," *Mater. Struct.*, vol. 27, pp. 563–571, Dec 1994, http://dx.doi.org/10.1007/BF02473124.

[29] M. Herbrand, A. Stark, and J. Hegger, "Size effect in unnotched concrete specimens in bedding: An analytical approach," *Struct. Concr.*, vol. 20, no. 2, pp. 660–669, Feb 2019, http://dx.doi.org/10.1002/suco.201800136.

[30] Z. P. Bažant and D. Novak, "Proposal for standard test of modulus of rupture of concrete with its size dependence," *ACI Mater. J.*, vol. 98, no. 1, pp. 79–87, Jan 2001.

[31] H. S. Müller and H. K. Hilsdorf, "Constitutive relations of structural concrete," *CEB Bullet. Inf.*, no. 217, pp. 17-65, Apr, 1993.

[32] K. Rokugo, Y. H. Katoh, and W. Koyanagi, "Fracture mechanics approach to evaluation of flexural strength of concrete," *ACI Mater. J.*, vol. 92, no. 5, pp. 561–566, Jan 1993.

Author contributions: JADFN: conceptualization, methodology, validation, data curation, formal analysis, writing – original draft; VGH: conceptualization, methodology, project administration, supervision, writing – review & editing.

Editors: Luís Oliveira Santos, Guilherme Aris Parsekian.